Comparative Analysis of Titanium Laser-Induced Plasma at Two Wavelengths Using Laser-Induced Breakdown Spectroscopy with Statistical Validation

Asmaa Mohammed Raoof[1], Jenan Abdullah Khlati[1], Muna Ahmed Issa[1], Shaymaa A. Hussein[2], Sami Salman Chiad[1], Nadir Fadhil Habubi[1,3,4] and Yassin Hasan Kadhim[5]
[1]*Department of Physics, College of Education, Mustansiriyah University, 10052 Baghdad, Iraq*
[2]*Department of Medical Laboratory Techniques, Al-Manara College for Medical Sciences, 62001 Amarah, Iraq*
[3]*Department of Radiation and Sonar Technologies, Alnukhba University College, 10001 Baghdad, Iraq*
[4]*Department of Radiology Techniques, Al-Qalam University College, 36001 Kirkuk, Iraq*
[5]*Department of Optics Techniques, College of Health and Medical Techniques, Al-Mustaqbal University, 51001 Hillah, Iraq*
dr.sami@uomustansiriyah.edu.iq

Keywords: LIBS, Titanium Plasma, Debye Length, Plasma Frequency, Nd:YAG Laser, 532 Nm, 1064 Nm, Optical Emission Spectroscopy, SPSS.

Abstract: In this work, we compare plasma characteristics when a pulsed Nd:YAG laser is focused at 532 nm and 1064 nm on the titanium target. At laser energies of 500 mJ and 700 mJ the plasma is measured by optical emission spectroscopy. Many plasma parameters including the temperature (calculated using Boltzmann plot) and electron density (calculated using Stark-broadened line profiles) will be obtained from the spectral lines of neutral titanium (i.e. Ti I). Some factors for Debye length (λ_D) and Debye number (N_D) have also been determined using the same laser spectroscopy in this paper. The 532 nm wavelength results in a higher electron density and plasma frequency, and the improved ionization efficiency is likely due to the increased photon energy. By contrast, at a 1064 nm wavelength, the electron temperature (Te) is higher, λD is longer, and the number of particles within the Debye sphere (ND) is greater due to more effective inverse bremsstrahlung absorption and thermal heating. The statistical measurements indicate that these differences and the observed wavelength variations depend strongly on the plasma's ionization parameters, and that 1064 nm shows higher thermal and collective plasma properties.

1 INTRODUCTION

Laser-induced breakdown spectroscopy (LIBS) is a versatile analytical technique for investigating the properties and elemental composition of various materials through the analysis of light emitted from laser-induced plasma [1]–[3]. Compared with many conventional elemental analysis techniques, LIBS is relatively simple to implement because it requires only a pulsed laser to generate a microplasma on the target surface [4]–[8]. The elemental composition of the sample is determined by analyzing the optical emission from the plasma plume [9]–[11]. During laser ablation, the absorbed laser energy causes melting and vaporization of the target material, leading to the formation of a plasma plume [12]–[16].

Optical emission spectroscopy (OES) is one of the most widely used diagnostic techniques for plasma characterization [17]–[19]. It provides an economical, versatile, and non-invasive method for diagnosing low-temperature and low-pressure plasmas [20]–[22]. OES has been extensively employed to determine key plasma parameters, such as electron temperature and electron density, in laser-induced plasmas [23]–[25].

Titanium was selected as the target material because of its high melting temperature [26], [27], strong interaction with laser radiation [28], [29], and well-defined emission lines [30], [31], which make it particularly suitable for plasma diagnostics using LIBS and OES. Therefore, this study aims to compare the characteristics of titanium plasma generated by a Nd laser operating at wavelengths of 532 nm and 1064 nm and to provide statistical validation of the obtained plasma parameters.

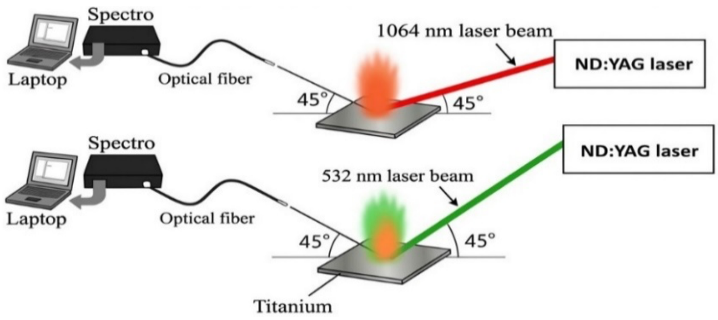

Figure 1: Diagram of the experimental setup of LIBS system.

2 EXPERIMENTAL

2.1 Experimental Setup and Data Acquisition

Our setup for the Nd:YAG laser operating at 532 nm and 1064 nm is shown in Figure 1. We conducted experiments at room temperature and normal atmospheric pressure under typical ambient conditions. The plasma was produced by firing pulses from the laser waveleght of (532 nm and 1064 nm). The laser pulses had energies of 500 mJ and 700 mJ. The pulse duration was 9 ns and the repetition frequency was 6 Hz. The titanium sheet was used as the test specimen, and the laser beam was focused on it at a 45-degree angle under atmospheric pressure. The optical emission light was collected and analyzed with a Surwit (S3000-UV-NIR) spectrometer using a 50 µm-core-diameter optical fiber, 1 cm away. Optical emission line data for the components were compared with the NIST database to determine plasma characteristics.

Statistical analysis of the measured plasma parameters was conducted to assess their reproducibility and stability. Using SPSS software, the mean values, standard deviations, and CV% were calculated for the two laser wavelengths and used to compare plasma emission. To determine the effect of laser wavelength on plasma emission behaviour, spectroscopic analyses and intensity-based calculations were carried out, as detailed in the following sections.

2.2 Spectral Intensity and Plasma Parameter Calculations

2.2.1 Spectral Intensity Determination

The emission intensity of the selected neutral titanium (Ti I) spectral lines was evaluated from the captured optical emission spectra using the spectrometer software. Peak intensity values were used to represent the emission strength of each spectral line. The same spectral lines and the same acquisition settings were used for both laser wavelengths to provide a reliable comparison.

2.2.2 Electron Temperature Calculation

Based on the assumption that the plasma maintains l ocal thermodynamic equilibrium, the Boltzmann Plo t method was used in the lab experiment to ascertain T_e [32]:

$$ln\left[\frac{\lambda_{ji} I_{ji}}{hcA_{ji}g_j}\right] = -\frac{1}{kT}(E_j) + ln\left|\frac{N}{U(T)}\right|. \quad (1)$$

Where g_{ji} is the degeneracy or statistical weight of the emitting upper level i of the studied transition, I_{ji} is the relative intensity of emission line between energy levels i and j, λ_{ji} is its wavelength, A_{ji} is the transition probability for spontaneous radiative emission from level i to lower level j, E_j is excitation energy of level i, k is Boltzmann constant, and N state population densities.

2.2.3 Electron Density Calculation

Electron density can be calculated using this equation [33].

$$n_e\,(cm^{-3}) = \left(\frac{\Delta\lambda}{2w_s}\right) N_r, \quad (2)$$

where Nr is the reference electron density, that is, equal to (1 x 10^{17}) cm^{-3}, and ω_s is the Stark broadening value obtained from the standard reference tables for the TiI emission line at 309 nm, used here as the calibrated reference transition for the Stark-broadening formalism rather than as one of the diagnostic lines measured in this experiment (444.9, 453.3, 461.7, 475.8, and 499.1 nm).

2.2.4 Derived Plasma Parameters:

Additional plasma properties were evaluated using the calculated T_e and density. The following formula was adopted to determine the plasma frequency (fp) [34], [35]:

$$f_p\ (\mathrm{Hz}) = 8.98\sqrt{n_e}. \quad (3)$$

The Debye length (λ_D) was calculated by applying [36], [37]:

$$\lambda_D\ (\mathrm{cm}) = 743\sqrt{\frac{T_e}{n_e}}. \quad (4)$$

The Debye number (N_D) was derived using [38], [39]:

$$N_D = \frac{4\pi}{3} n_e \lambda_D^3. \quad (5)$$

2.2.5 Statistical Analysis

The statistical data on plasma parameters were analysed using SPSS. To assess the dataset's quality, descriptive statistics were computed, including mean and standard deviation. The results for plasma parameters were presented as the coefficient of variation (CV%) and the absolute difference (Δ) at the two different laser wavelengths.

The coefficient of variation was calculated by the formula [40]:

$$\mathrm{CV\%} = (\mathrm{SD} / \mathrm{Mean}) \times 100. \quad (6)$$

The absolute difference was calculated as follows [41] to assess the degree and direction of variation among the plasma parameters at various laser wavelengths:

$$\Delta = X_{1064} - X_{532}. \quad (7)$$

The mean values of the plasma parameters at lase r wavelengths of 1064 nm and 532 nm, respectively, are shown by X_{1064} and X_{532}.

3 RESULTS AND DISCUSSION

3.1 Comparison of OES at Different Laser Wavelengths:

As far as the spectral features appear to confirm the neutral titanium (i.e. Ti I) and very few lines of ionized titanium (i.e., Ti II), we could find the same in the UV radiation (see Fig. 2 and 3). This means that at these extreme energetic plasma or excitation levels, neutral species are available, while Ti II peaks should be present because ionization can occur at high energies.

With increasing laser energy from 500 mJ to 700 mJ, the emission intensity increased significantly, with a very strong enhancement in both plasma excitation and ablation ability. In addition, even at lower laser energy, the total emission and peak intensity increased with laser wavelength, particularly in the ultraviolet-visible region, with the highest emission intensity coming from neutral titanium (Ti I). This was because, with higher laser energy, an energy density builds up at the target surface, material is removed (ablation), and excited species are produced in the plasma [42]. In our study, we found that the plasma light concentration from a 532 nm laser pulse is higher than that from a 1064 nm laser pulse, as previously reported. This was due to the greater photon energy at shorter wavelengths, which led to greater absorption of energy by the target, producing a more attractive plasma beam at shorter wavelengths [43]. A detailed investigation of the observed emission intensity at 532 nm also shows the strong relationship between an increase in the photon's energy density and an improved excitation efficiency in the laser [44]. Thus, a larger population and a greater number of excited atoms and ionic species can be considered sources [45].

3.2 Comparison of Electron Temperature at Different Laser Wavelengths

In this work, T_e of a laser-generated titanium plasma is calculated from emission lines of neutral titanium (Ti I) using Boltzmann plots. In order to create the Boltzmann plot, the most prominent and properly specified spectral lines are used, based on which the overall yield is better known. As a result, we use four emission lines for the plasma generated by the 532 nm laser, while five lines are used for the plasma generated by the 1064 nm laser. Table 1: Spectroscopic parameters for the Ti I lines selected were of wavelength λ, transition probability g_kA_{ki} and energy of upper and lower levels E_j and E_i. We compared laser excitations with the titanium T_e from 532 nm and 1064 nm (at 1064 nm) as well. This approach can be used to determine T_e, as the emission energy levels of Ti I are identical; the differences in temperature obtained from the plasma light spectrum are mainly determined by the laser wavelength [46], [47].

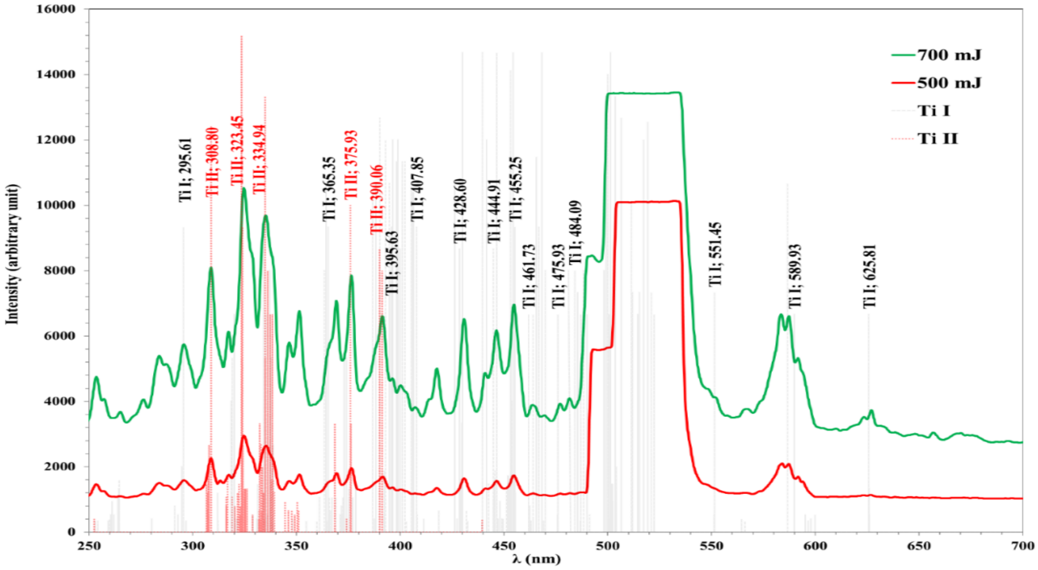

Figure 2: The emission spectra of Titanium plasma for a 532 nm wavelength.

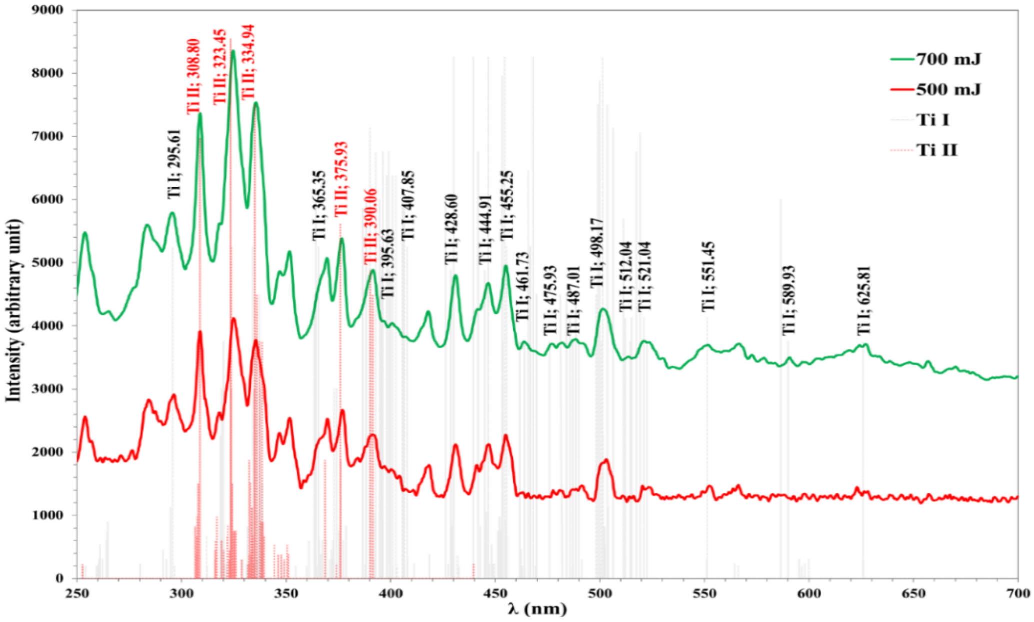

Figure 3: The emission spectra of Titanium plasma for a 1064 nm wavelength.

Table 1: Spectroscopic parameters of selected Ti I emission lines used for 532 nm and 1064 nm.

Wavelength	gkAki	Ei	Ej
444.9143	1.1e+09	1.887	4.67301
453.3240	9.71e+08	0.848	3.58265
461.7268	7.66e+08	1.749	4.43335
475.8118	7.84e+08	2.249	4.85424
499.1067	6.42e+08	0.836	3.31943

Images of Boltzmann plots of the Ti I emission lines at the two laser wavelengths shown in Figures 4 and 5 are presented. Using the current equation in (1), T_e can be determined from the slope of the regression line in the Boltzmann plot: the slope of the logarithm of the normalized line strength corresponds to the associated upper energy level. One sees a clearly linear trend in the Boltzmann plots of these lines in the upper graph of the plasma, leading to local thermodynamic equilibrium (LTE), so we see this was effective in determining T_e, as a matter of fact [48], [49].

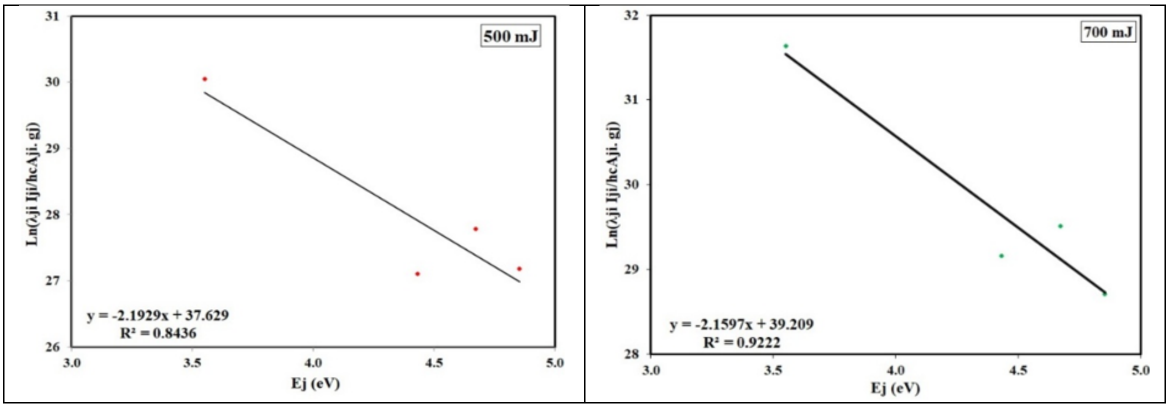

Figure 4: Boltzmann plot for Ti plasma at laser energy 500-700 mJ using λ 532 mm.

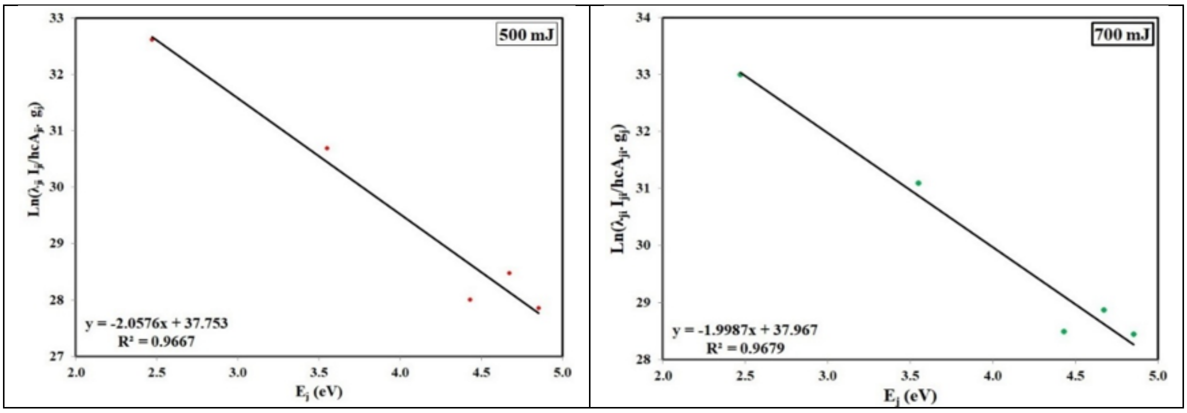

Figure 5: Boltzmann plot for Ti plasma at laser energy 500-700 mJ using λ 1064 mm.

We find that for a laser energy of 500 mJ, the Boltzmann plot of the plasma produced at 532 nm has a somewhat steeper slope than that of the plasma at 1064 nm, since the electron temperature drops (Fig. 5). This observation relates to the fact that, across different wavelength ranges with this system, the Boltzmann plot has a negative slope, since the thermal population of excited states is lowest at 532 nm [50]. The plasma energy pattern at 700 mJ increases with laser energy until we reach 700 mJ; however, the plasma generated at 1064 nm has a shallower negative slope, suggesting a higher electron temperature than at 532 nm. It can be argued that a longer wavelength is better at carrying energy from the plasma, but much of the excitation is due to thermal excitation at higher energies [51]. Additionally, the coefficient of determination (R^2) of the Boltzmann plots increases with laser energy for both wavelengths, indicating greater linearity at 700 mJ and, therefore, a better fit of the experimental data [52]. Also, at 700 mJ, the plasma R^2 values are similar and close to 1, indicating that the plasma approaches local thermodynamic equilibrium (LTE) [53].

In Tables 2 and 3 T_e is higher at 1064 nm with laser wavelength as compared to 532 nm, and this is also predicted from previous work [54], which shows that for a laser energy of 500 mJ, the electron temperature increases from 0.456 eV at 532 nm to 0.486 eV at 1064 nm. In this case, we have a laser energy of 700 mJ, with electron temperatures of 0.500 eV at 1064 nm and 0.463 eV at 532 nm. The electron temperature rise is related to the stronger coupling to energy at longer wavelengths, but our laser operates at 1064 nm, which is faster: the inverse bremsstrahlung is absorbed in the plasma and therefore transfers more energy to the free electrons. To this end, electron heating and temperatures increase at longer wavelengths [55].

3.3 Comparison of Electron Density at Different Laser Wavelengths

In Figures 6 and 7, we show that as the laser energy increases from 500 mJ to 700 mJ, the spectral line width widens. Thus, the electron density in the plasma increases with this. Also, the spectral linewidth in 532 nm is much broader than that in 1064 nm, as shown in Tables 2 and 3. This shows that the plasma contains a high number of electrons at a much shorter wavelength, in agreement with earlier studies [56]. The widening of spectral lines is due to the Stark effect. At high electron density, electrons interact more with the emitting particles or atoms. As such, a broad linewidth at 532 nm indicates a high number of plasma-generated charges interacting with the emitting species, thereby affecting the energy levels of the radiating atoms and ions. The relatively thinner linewidth at 1064 nm suggests that the electron density is lower and that collisional broadening will have less effect during the same experiments.

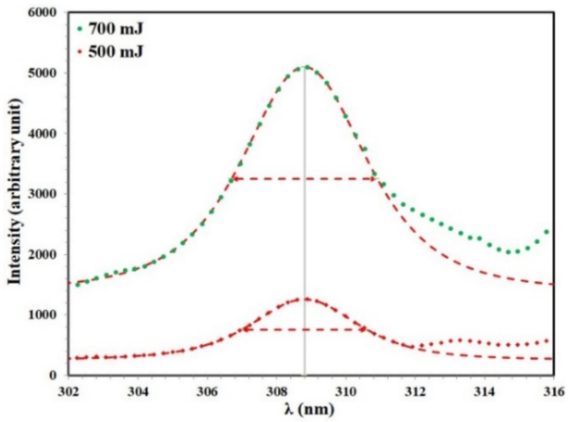

Figure 6: Gaussian fitting of the 532 nm wavelength.

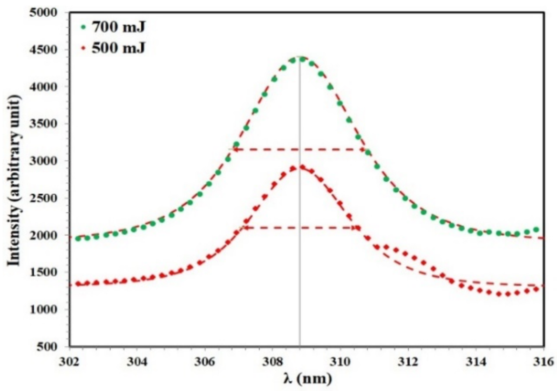

Figure 7: Gaussian fitting of the 1046 nm wavelength.

The effect of laser wavelength on plasma characteristics is highlighted in Figures 8 and 9. We discovered that a 532 nm laser yields higher electron temperature and density than a 1064 nm laser because its absorbed spectrum is shorter and it interacts more effectively with the target material at shorter wavelengths. In other words, the longer-wavelength photons make the plasma more ablated on the top, and less energy can be produced at the bottom, where the bottom particles are created. This results in a larger number of excited and free electrons and thus higher T_e and density than with the laser's longer-wavelength 1064 nm light.

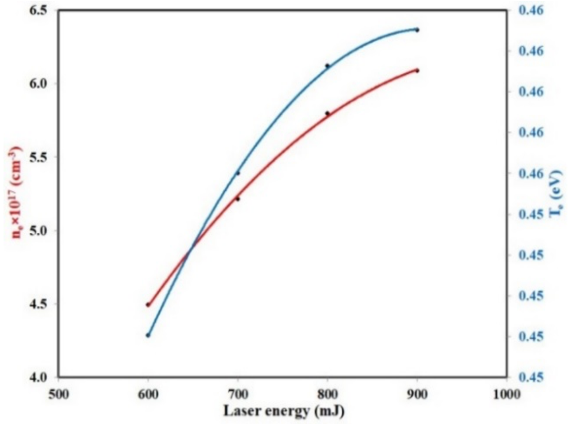

Figure 8: The relation between T_e and n_e with energy for a 532 nm wavelength.

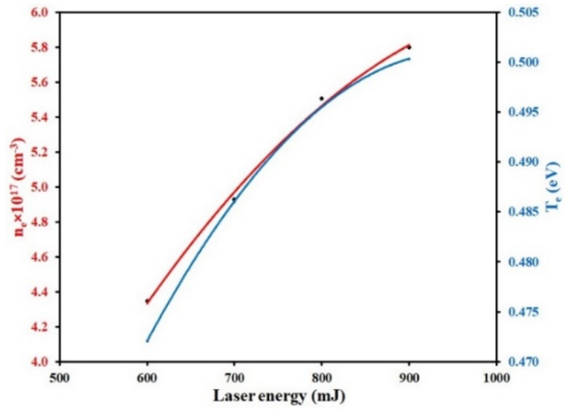

Figure 9: The relation between T_e and n_e with energy for a 1064 nm wavelength.

3.4 Comparison of Derived Plasma Parameters at Different Laser Wavelengths

When the electron density increases with temperature, we can compute f_p, λ_D, and N_D as in (3), (4), and (5). As predicted, the electron density increases with the plasma frequency, and, as we have shown in Tables 2 and 3, it does so directly. The plasma frequency at 532 nm is higher than that at 1064 nm, due to the higher electron density at a shorter wavelength. Since f_p is proportional to the square root of the electron density, higher ionization at 532 nm results in a higher plasma frequency [57].

The Debye length is influenced directly by T_e and inversely by the electron density [58]. As a result, the longer-wavelength 1064 nm laser produces a lower electron density, resulting in a longer Debye length. In addition, the number of particles inside the Debye sphere in Tables 2 and 3 is higher at 1064 nm than at 532 nm (i.e., the total Debye length is higher). In summary, changing the wavelength to 1064 nm improves some plasma properties (especially λ_D and N_D), where a shorter wavelength yields a higher electron density but a higher plasma frequency.

Table 2: Plasma parameter for 532 nm wavelength.

E (mJ)	T_e (eV)	$n_e \times 10^{17}$ (cm^{-3})	$f_p \times 10^{10}$ (Hz)	$\lambda_D \times 10^{-5}$ (cm)	N_D
500	0.456	5.217	648.639	0.695	732
700	0.463	6.087	700.610	0.648	694

Table 3: Plasma parameter for 1064 nm wavelength.

E (mJ)	T_e (eV)	$n_e \times 10^{17}$ (cm^{-3})	$f_p \times 10^{10}$ (Hz)	$\lambda_D \times 10^{-5}$ (cm)	N_D
500	0.486	4.928	630.364	0.738	829
700	0.500	5.797	683.726	0.690	799

3.5 Statistical Comparison of Plasma Parameters at Different Laser Wavelengths

3.5.1 Comparison Based on Mean Values and Standard Deviation

We first conducted several statistical tests, which included average and mean values for both laser wavelengths (532 and 1064 nm for the plasma). Statistics are presented in Table 4, and the analysis shows that, in the plasma, the average values at both wavelengths differ significantly, as evidenced by the statistical tests. The plasma (at 532 nm) has a higher density and plasma frequency. We expect more effective ionization and the low standard deviations of these results make them reliable and reproducible. In the plasma obtained at 1064 nm, we observe a higher electron temperature, an increased λ_D, and N_D. These two features are significantly affected by the thermal energy of the electrons [59].

The relationship between the physical characteristics of plasma and the statistical analyses shows that the variations observed in plasma parameters result from genuine effects linked to the laser wavelength, rather than random fluctuations. Hence, the differences in plasma behavior that depend on the wavelength are significant both statistically and in terms of their physical meaning [60].

3.5.2 Statistical Assessment of Plasma Parameters Using Absolute Difference and Coefficient of Variation

To verify the observed behaviour of the plasma, we have calculated the absolute differential (Δ) between plasma parameters at 532 nm and 1064 nm in Fig 10a, b and Table 5. Positive Δ values of the electron temperature, λ_D, and N_D indicate that these parameters are higher at 1064 nm [61]. On the other hand, negative Δ values for electron density and plasma frequency indicate that the parameters related to ionization are higher at 532 nm.

This is consistent with our observations shown in Figure 10. They are evident in our plasma emission spectra: better ionization efficiency at the shorter wavelength and better thermal and screening effects at the longer wavelength [62]. Still, we expect that photons of short wavelength are absorbed by electrons, not by electrons in a thicker plasma, as with photons of long wavelength. In this case, as we are only using a short-wavelength laser (532 nm), the laser itself provides more efficient ionization and thus a much denser plasma (hence the increased density). And the laser with a longer wavelength (1064 nm) provides energy more slowly. Hence, the electron thermal behavior is more favorable, λ_D is maximized, N_D increases. These results confirm that plasma parameters are controlled by the laser wavelength, not by random variation. The laser wavelength is an essential parameter that characterizes the properties of ionized and thermal plasmas [63].

Figure 11 and Table 6 show the coefficient of variation and plasma volume at 532 nm and 1064 nm laser wavelengths. We find that plasma at 532 nm exhibits low variability in radiation and plasma frequency, and greater uniformity when ionizing particles. This may be related to the higher energy of the 532 nm laser, which excites and ionizes atoms, thus forming a dense plasma with an even number of atoms. Furthermore, Debye-related parameters, e.g., the Debye length and the particle number within one Debye sphere, are more stable at 1064 nm.

Consequently, the variation coefficient not only assesses parameter stability but also reflects the mechanism of plasma formation by wavelength: shorter wavelengths yield more reproducible ionization, while longer wavelengths favour stable thermal/electrostatic properties [64].

Table 4: The mean and S.D for 532 and 1064 nm wavelength.

Parameter	532 nm (Mean ± SD)	1064 nm (Mean ± SD)
Electron temperature (eV)	0.4595 ± 0.0050	0.4930 ± 0.0099
Electron density $\times 10^{17}$ (cm^{-3})	5.6520 ± 0.6518	5.3625 ± 0.6145
Plasma frequency $\times 10^{10}$ (Hz)	674.625 ± 36.749	657.045 ± 37.733
Debye length$\times 10^{-5}$ (cm)	0.6715 ± 0.0332	0.7140 ± 0.0339
Debye number	713 ± 27	814 ± 21

Table 5: The absolute difference (Δ) between the wavelengths of 532 nm and 1064 nm.

Plasma parameter	Unit	Mean at 532 nm	Mean at 1064 nm	Δ (1064 − 532)
Electron temperature (T_e)	eV	0.4595	0.4930	+0.0335
Electron density (n_e)	$\times 10^{17}$ cm^{-3}	5.6520	5.3625	−0.2895
Plasma frequency (f_p)	$\times 10^{10}$ Hz	674.625	657.045	−17.580
Debye length (λ_D)	$\times 10^{-5}$ cm	0.6715	0.7140	+0.0425
Debye number (N_D)	-	713	814	+101

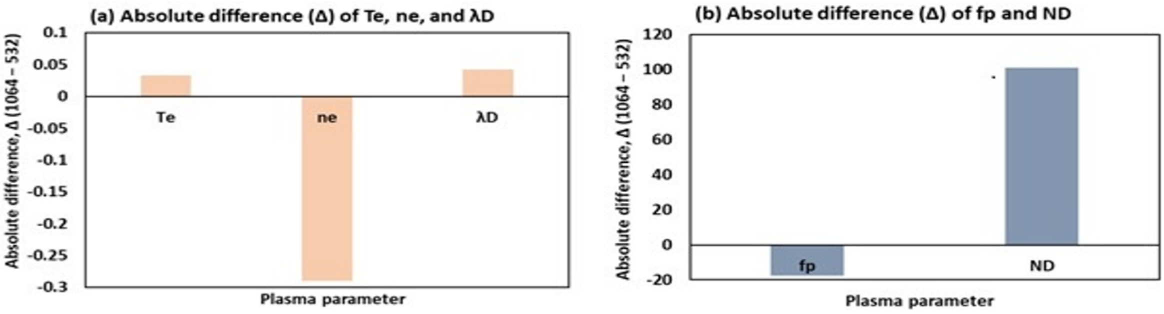

Figure 10: Absolute difference of plasma parameter.

Table 6: (CV%) for 532 and 1064 nm wavelengths.

Parameter	CV% at 532 nm	CV% at 1064 nm	More stable
T_e	1.09 %	2.01 %	532 nm
n_e	11.54 %	11.46 %	1064 nm
f_p	5.44 %	5.74 %	532 nm
λ_D	4.95 %	4.75 %	1064 nm
N_D	3.77 %	2.60 %	1064 nm

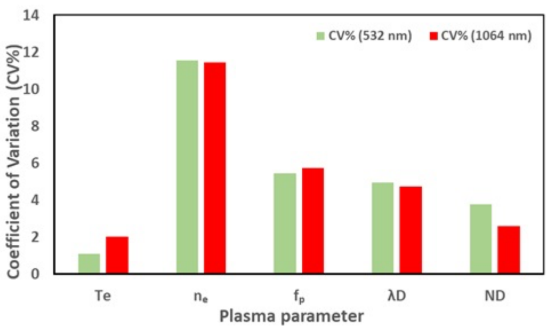

Figure 11: The coefficient of variation (CV%) for plasma parameters at laser wavelengths of 532 and 1064 nm.

4 CONCLUSIONS

The results and statistics have indicated that the laser wavelength plays an important role in revealing the features of the laser-induced Titanium plasma. With a shorter wavelength of 532 nm, the electrons are ionized more efficiently, leading to much larger electron densities and, therefore, higher plasma frequencies at shorter wavelengths compared to longer wavelengths. Because photons at a shorter wavelength, 532 nm, have more energy, we achieve greater excitation and ionization in a given target material. However, the longer wavelength of 1064 nm also increases the laser's interaction with plasma electrons via inverse bremsstrahlung, thereby naturally increasing the electron temperature. Such a thermal advantage between 1064 nm and 532 nm corresponds to a longer Debye length, more particles within the Debye sphere, and, therefore, a plasma with stronger collective and screening behavior. However, using statistical measures such as the mean and standard deviation, absolute differences, and the coefficient of variation, we find that these changes are largely due to random fluctuations, whereas the laser wavelength increases the total number of particles in the Debye. Our 532 nm laser generates ionization radiation, while the 1064 nm laser yields a plasma with better thermal and collective behavior [65], [66].

ACKNOWLEDGMENTS

The authors acknowledge the support of the academic research program at Mustansiriyah University (www.uomustansiriyah.edu.iq) for supporting this study.

REFERENCES

[1] M. Mehdizadeh, A. Omidi, T. M. Ikegwu, C. A. Okolo, E. I. IfedibaluChukwu, and L. C. Ndufeiya-Kumasi, "Laser-Induced Breakdown Spectroscopy (LIBS) for Rapid Food Safety Monitoring: Advancements, Applications, and Future Directions," Food Safety and Health, vol. 4, no. 1, pp. 50-66, 2026.

[2] M. Vasudeva, S. D. Varalakshmi, S. D. George, and V. K. Unnikrishnan, "Engineered liquid-repellent substrate for enhanced Laser-Induced Breakdown Spectroscopy (LIBS) of liquid samples," Applied Surface Science, vol. 166364, 2026.

[3] M. Rizwan, M. S. Afgan, S. Saleem, Z. Hou, and Z. Wang, "Influence of Key Parameters on Signal Quality in Double-Pulse Laser Induced Breakdown Spectroscopy (DP-LIBS)," Journal of Analytical Atomic Spectrometry, 2026.

[4] B. Chen, B. Starman, M. Halilovič, L. A. Berglund, and S. Coppieters, "Finite element model updating for material model calibration: A review and guide to practice," Archives of Computational Methods in Engineering, vol. 32, no. 4, pp. 2035-2112, 2025.

[5] T. Xu, Y. Pan, Z. Shen, L. Shen, C. Dong, G. Zhang, and J. Lu, "Ablation mechanism of porous silicon nitride irradiated by continuous wave laser under tangential gas flow," Journal of the American Ceramic Society, vol. 109, no. 1, p. e70496, 2026.

[6] M. Nadeem, M. Faheem, M. Manzoor, A. Gulzar, M. Bilal, and Y. Jamil, "Machine learning assisted LIBS classification of burnt and unburnt paper samples: A forensic perspective," Talanta, vol. 293, p. 128073, 2025.

[7] D. Zhang, H. Ma, J. Nie, Y. Liu, and L. Guo, "A spectral bias-error stepwise correction method of plasma image-spectrum fusion based on deep learning for improving the performance of LIBS," Talanta, vol. 281, p. 126872, 2025.

[8] C. W. Schneider and T. Lippert, "PLD plasma plume analysis: A summary of the PSI contribution," Applied Physics A, vol. 129, no. 2, p. 138, 2023.

[9] M. Mohan, D. Prochazka, Y. You, J. Riedel, I. Gornushkin, I. Ročňáková, and J. Kaiser, "Investigating plasma morphology at material boundaries under varying ambient pressures," Talanta, vol. 295, p. 128377, 2025.

[10] N. Ajamgard, A. Chehrghani, M. J. Sobhani, M. J. Torkamany, and A. Ghorbanzadeh, "In-situ determination of micro-hardness in laser cladding of stellite using optical emission spectroscopy," Optics & Laser Technology, vol. 177, p. 111058, 2024.

[11] M. A. Issa and K. A. Aadim, "Influence Of Laser Energy On Structural And Optical Properties Of ZnO(x):NiO(1−x) Films Prepared By Pulse Laser Deposition," Journal of Optics, 2024, [Online]. Available: https://doi.org/10.1007/s12596-024-02212-2.

[12] A. Palla-Papavlu, A. Bercea, M. O. Cernaianu, V. Marascu, B. Butoi, C. Porosnicu, and G. Dinescu, "Nanosecond laser interaction with Beryllium: study of surface erosion and material removal dynamics," Materials & Design, p. 114916, 2025.

[13] N. A. Inogamov, Y. V. Petrov, V. A. Khokhlov, and V. V. Zhakhovskii, "Laser ablation: physical concepts and applications," High Temperature, vol. 58, no. 4, pp. 632-646, 2020.

[14] H. Naser, M. A. Alghoul, M. K. Hossain, N. Asim, M. F. Abdullah, M. S. Ali, and N. Amin, "The role of laser ablation technique parameters in synthesis of nanoparticles from different target types," Journal of Nanoparticle Research, vol. 21, no. 11, p. 249, 2019.

[15] N. Ali, S. Bashir, A. M. Alshehri, and N. Begum, "Study of micro/nano structuring and mechanical properties of KrF excimer laser irradiated Al for aerospace industry and surface engineering applications," Materials, vol. 14, no. 13, p. 3671, 2021.

[16] J. Zhang, J. Claverie, M. Chaker, and D. Ma, "Colloidal metal nanoparticles prepared by laser ablation and their applications," ChemPhysChem, vol. 18, no. 9, pp. 986-1006, 2017.

[17] H. O. Hussein and W. I. Yaseen, "Plasma optical emission spectroscopy study of some iron meteorites," Iraqi Journal of Science, pp. 2925-2933, 2024.

[18] M. A. Issa and K. A. Aadim, "Optical and structural characterization of ZnO:NiO nano composite prepared by pulsed laser deposition method," Journal of Optics, vol. 54, pp. 2357-2362, 2025, [Online]. Available: https://doi.org/10.1007/s12596-024-01951-6.

[19] S. M. Fathi and S. J. Kadhim, "Optical emission spectroscopy for studying Fe plasma parameters produced by exploding wire technique in carbon nanotubes-water colloid," Iraqi Journal of Science, pp. 163-169, 2022.

[20] P. Purohit, F. J. Fortes, and J. J. Laserna, "Optical trapping as a morphologically selective tool for in situ LIBS elemental characterization of single nanoparticles generated by laser ablation of bulk targets in air," Analytical Chemistry, vol. 93, no. 4, pp. 2635-2643, 2021.

[21] H. M. Roomy and H. H. Murbat, "Evaluate the argon plasma jet parameters by optical emission spectroscopy," Kuwait Journal of Science, vol. 50, no. 2, pp. 163-167, 2023.

[22] E. H. Kwapis, J. Borrero, K. S. Latty, H. B. Andrews, S. S. Phongikaroon, and K. C. Hartig, "Laser ablation plasmas and spectroscopy for nuclear applications," Applied Spectroscopy, vol. 78, no. 1, pp. 9-55, 2024.

[23] G. D. Förster and L. J. Lewis, "Numerical study of double-pulse laser ablation of Al," Physical Review B, vol. 97, no. 22, p. 224301, 2018.

[24] T. U. Rahman, Z. U. Rehman, S. Ullah, H. Qayyum, B. Shafique, R. Ali, and A. Qayyum, "Laser-induced plasma-assisted ablation (LIPAA) of glass: Effects of the laser fluence on plasma parameters and crater morphology," Optics & Laser Technology, vol. 120, p. 105768, 2019.

[25] M. A. Issa and K. A. Aadim, "Study the structural and optical properties of Zinc Oxide prepared by pulse laser deposition," Journal of Optics, vol. 55, pp. 755-760, 2026, [Online]. Available: https://doi.org/10.1007/s12596-024-02034-2.

[26] Ahmed, Q. Nan, W. Akhtar, S. Mubashir, D. Yang, L. Yong, and Z. Jingchuan, "Prediction of low-modulus Ti-based refractory high-entropy alloys for orthopedic implants using machine learning and DFT calculations," Physica B: Condensed Matter, vol. 715, p. 417560, 2025.

[27] G. Qian, H. Wang, S. Pang, Y. Sun, J. Guo, D. Wang, and Z. Wang, "New insights into the application of non consumable electrode electroslag remelting refining: Enhanced removal of inclusions in Ti-Si alloy based the reduction of Ti-bearing blast furnace slag by SoG-Si scraps," Journal of Cleaner Production, vol. 490, p. 144684, 2025.

[28] H. Liang, S. Zhang, R. Zhang, H. Zhou, L. Xia, Y. Sun, and H. Wang, "Strong interaction between Fe and Ti compositions for effective CO2 hydrogenation to light olefins," Chinese Journal of Catalysis, vol. 71, pp. 146-157, 2025.

[29] V. Lapidas, A. B. Cherepakhin, A. G. Kozlov, A. V. Shevlyagin, K. Kolonica, S. Shevlyagina, and A. A. Kuchmizhak, "Structural coloration on titanium films by direct femtosecond laser patterning empowered by neural networks," ACS Applied Materials & Interfaces, vol. 17, no. 10, pp. 16122-16131, 2025.

[30] R. Zhang, X. Li, Y. Liu, X. Mao, Y. Wei, Y. Wang, and J. Jia, "Surface aging of Ti-based MXene attenuates mitochondrial toxicity via suppressed cellular uptake and reactivity," Environmental Pollution, vol. 395, p. 127793, 2026.

[31] S. C. Shit, D. Kwon, N. T. Y. Phan, H. W. Kim, J. Park, J. H. Lee, and W. Kim, "Ni Single-Atom Modulation of Ti-O Covalency Boosts Ammonia Oxidation Electrocatalysis," Advanced Science, p. e21932, 2026.

[32] Mrotzek and W. Viöl, "Spectroscopic characterization of an atmospheric pressure plasma jet used for cold plasma spraying," Applied Sciences, vol. 12, no. 13, p. 6814, 2022.

[33] M. Issa and K. A. Aadim, "Influence of gas flow rate on the plasma temperature and electron density of an atmospheric argon plasma jet," Jordan Journal of Physics, vol. 18, no. 4, pp. 435-442, 2025.

[34] H. M. Abdulwahab and H. R. Humud, "Plasma characterization of microwave plasma jet at Atmospheric pressure," Iraqi Journal of Science, pp. 151-159, 2024.

[35] M. H. Ahmed and H. R. Humud, "The Influence of Gas Type and Flow Rate on Plasma Jet Length and Gas Temperature," Iraqi Journal of Physics, vol. 23, no. 3, pp. 128-136, 2025.

[36] A. A. Hussain, "Plasma characteristics of Ag: Al alloy produced by fundamental and second harmonic frequencies of Nd: YAG laser," Iraqi Journal of Physics, vol. 14, no. 31, pp. 205-214, 2016.

[37] Q. A. Abbas, A. F. Ahmed, and F. A. H. Mutlak, "Spectroscopic analysis of magnetized hollow cathode discharge plasma characteristics," Optik, vol. 242, p. 167260, 2021.

[38] D. K. Naser and M. J. Kadhim, "Diagnostics of tin and cadmium plasma produced by laser Nd: YAG (1064 nm)," in AIP Conference Proceedings, vol. 2839, no. 1, p. 080015, 2023.

[39] A. S. Wasfi, H. R. Humud, and N. K. Fadhil, "Synthesis of core-shell Fe3O4-Au nanoparticles by electrical exploding wire technique combined with laser pulse shooting," Optics & Laser Technology, vol. 111, pp. 720-726, 2019.

[40] A. Canchola, S. Tang, P. Hemyari, E. Paxinos, and E. Marins, "Correct use of percent coefficient of variation (% CV) formula for log-transformed data," MOJ Proteomics & Bioinformatics, vol. 6, no. 4, pp. 10-15406, 2017.

[41] F. Bensch, J. Stutzki, and V. Ossenkopf, "Quantification of molecular cloud structure using the Δ-variance," Astronomy & Astrophysics, vol. 366, no. 2, pp. 636-650, 2001.

[42] A. E. Hussein, P. K. Diwakar, S. S. Harilal, and A. Hassanein, "The role of laser wavelength on plasma generation and expansion of ablation plumes in air," Journal of Applied Physics, vol. 113, no. 14, 2013.

[43] N. M. Shaikh, M. S. Kalhoro, A. Hussain, and M. A. Baig, "Spectroscopic study of a lead plasma produced by the 1064 nm, 532 nm and 355 nm of a Nd:YAG laser," Spectrochimica Acta Part B: Atomic Spectroscopy, vol. 88, pp. 198-202, 2013.

[44] J. Hu, W. Li, D. Li, H. Liu, N. Xia, T. Zhang, and Z. Wang, "High-Power, High-Beam-Quality, Long-Pulse-Width 532 nm Laser Based on a 4f Optical System," Applied Sciences, vol. 14, no. 21, p. 9620, 2024.

[45] H. Liu, Q. Li, Y. Ding, X. Liu, J. Hu, B. Yang, and Z. Wang, "High-beam-quality and high-brightness 532 nm laser with output power 96 W," Crystals, vol. 13, no. 2, p. 290, 2023.

[46] A. Issa and K. A. Aadim, "Activity of (ZnO:NiO) nanoparticles prepared by plasma jet and pulse laser deposition (PLD) techniques against Staphylococcus aureus, Staphylococcus epidermidis, Klebsiella species, Escherichia coli and Candida albicans," in AIP Conference Proceedings, vol. 3415, no. 1, p. 030004, 2026.

[47] G. Mauer and E. J. Gildersleeve V, "Using optical emission spectroscopy in atmospheric conditions to track the inflight reduction of plasma sprayed TiO2-x feedstock for thermoelectric applications," Scientific Reports, vol. 14, no. 1, p. 554, 2024.

[48] X. Hu, H. Wu, D. Wu, X. Wang, S. Liu, K. Xu, and H. Ding, "Dynamics of laser-ablated molybdenum plasma in vacuum: a novel spectral matching algorithm based on Saha-Boltzmann equilibrium for ne and Te determination in fusion wall diagnostics," Journal of Analytical Atomic Spectrometry, vol. 40, no. 9, pp. 2362-2372, 2025.

[49] H. B. Andrews, L. R. Sadergaski, and K. G. Myhre, "Neptunium transition probabilities estimated through laser induced breakdown spectroscopy (LIBS) measurements," Journal of Analytical Atomic Spectrometry, vol. 37, no. 4, pp. 768-774, 2022.

[50] B. Bousquet, V. Gardette, V. M. Ros, R. Gaudiuso, M. Dell'Aglio, and A. De Giacomo, "Plasma excitation temperature obtained with Boltzmann plot method: Significance, precision, trueness and accuracy," Spectrochimica Acta Part B: Atomic Spectroscopy, vol. 204, p. 106686, 2023.

[51] S. Nijdam, K. V. Desai, S. J. Park, P. P. Sun, O. Sakai, G. Lister, and J. G. Eden, "Foundations of plasma photonics: lamps, lasers, and electromagnetic devices," Plasma Sources Science and Technology, vol. 31, no. 12, p. 123001, 2022.

[52] M. John and K. K. Anoop, "A numerical procedure for understanding the self-absorption effects in laser induced breakdown spectroscopy," RSC Advances, vol. 13, no. 42, pp. 29613-29624, 2023.

[53] A. Issa and K. A. Aadim, "Optical Emission Spectroscopy of Zinc Oxide Doped Nickel Oxide to Calculate Plasma Parameters Using the Boltzmann Plot Method," Iraqi Journal of Physics, vol. 23, no. 2, pp. 118-127, 2025.

[54] T. A. Khalepha and N. K. Abdalameer, "Comparative analysis of plasma generated using LIBS technique for different wavelengths of pulsed laser of a cadmium target," Baghdad Science Journal, vol. 21, no. 12 (Suppl.), pp. 4128-4139, 2024.

[55] Adamovich, S. D. Baalrud, A. Bogaerts, P. J. Bruggeman, M. Cappelli, V. Colombo, and A. Vardelle, "The 2017 Plasma Roadmap: Low temperature plasma science and technology," Journal of Physics D: Applied Physics, vol. 50, no. 32, p. 323001, 2017.

[56] M. Asif, U. Amin, Z. U. Rehman, R. Ali, and H. Qayyum, "Characterization of the palladium plasma produced by nanosecond pulsed 532 nm and 1064 nm wavelength lasers," Laser Physics, vol. 32, no. 2, p. 026002, 2022.

[57] M. Musadiq, N. Amin, Y. Jamil, M. Iqbal, M. A. Naeem, and H. A. Shahzad, "Measurement of electron number density and electron temperature of laser-induced silver plasma," International Journal of Engineering & Technology, vol. 2, no. 1, p. 32, 2013.

[58] M. J. Huang, T. M. Chang, C. K. Liu, and C. K. Yu, "A theoretical study of the specific heat and Debye temperature of low-dimensional materials," International Journal of Heat and Mass Transfer, vol. 51, no. 17-18, pp. 4470-4479, 2008.

[59] S. Raju, "A thermophysical perspective of the inter-relationship between Debye temperature and electron density," Metallurgical and Materials Transactions A, vol. 52, no. 1, pp. 242-256, 2021.

[60] M. A. Khadim, H. R. Humud, and S. J. Ali, "Optical emission spectroscopy of laser-produced nickel plasma in different ambient gases," Plasma Science and Technology, vol. 24, no. 5, p. 055401, 2022.

[61] D. W. Hahn and N. Omenetto, "Laser-induced breakdown spectroscopy (LIBS), part II: review of instrumental and methodological approaches to material analysis and applications to different fields," Applied Spectroscopy, vol. 66, no. 4, pp. 347-419, 2012.

[62] A. De Giacomo, M. Dell'Aglio, R. Gaudiuso, G. Cristoforetti, S. Legnaioli, V. Palleschi, and E. Tognoni, "Spatial distribution of hydrogen and other emitters in aluminum laser-induced plasma in air and consequences on spatially integrated laser-induced breakdown spectroscopy measurements," Spectrochimica Acta Part B: Atomic Spectroscopy, vol. 63, no. 9, pp. 980-987, 2008.

[63] P. Singh and S. N. Thakur, Eds., "Laser-Induced Breakdown Spectroscopy", Amsterdam, Netherlands: Elsevier, 2007.

[64] D. A. Cremers and L. J. Radziemski, *Handbook of Laser-Induced Breakdown Spectroscopy*, 2nd ed. Chichester, U.K.: Wiley, 2013.

[65] A. Canchola, S. Tang, P. Hemyari, E. Paxinos, and E. Marins, "Correct use of percent coefficient of variation (% CV) formula for log-transformed data," MOJ Proteomics & Bioinformatics, vol. 6, no. 4, pp. 10-15406, 2017.

[66] R. K. Aldubhani, H. R. Humud, and A. F. Ahmed, "Spectroscopic diagnostics of laser-induced plasma generated from aluminum target in different background gases," Optics & Laser Technology, vol. 185, p. 112943, 2026.